
This copy is for your personal, non-commercial use only.

If you wish to distribute this article to others, you can order high-quality copies for your colleagues, clients, or customers by [clicking here](#).

Permission to republish or repurpose articles or portions of articles can be obtained by following the guidelines [here](#).

The following resources related to this article are available online at www.sciencemag.org (this information is current as of October 28, 2014):

Updated information and services, including high-resolution figures, can be found in the online version of this article at:

<http://www.sciencemag.org/content/339/6125/1328.full.html>

Supporting Online Material can be found at:

<http://www.sciencemag.org/content/suppl/2013/01/30/science.1230593.DC1.html>

This article **cites 52 articles**, 23 of which can be accessed free:

<http://www.sciencemag.org/content/339/6125/1328.full.html#ref-list-1>

This article has been **cited by** 10 articles hosted by HighWire Press; see:

<http://www.sciencemag.org/content/339/6125/1328.full.html#related-urls>

This article appears in the following **subject collections**:

Cell Biology

http://www.sciencemag.org/cgi/collection/cell_biol

cell settings, insulin acutely stimulated an increase in labeling of intermediates in pyrimidine synthesis in G9C cells expressing wild-type CAD, and this was blocked by the S6K1 inhibitor (Fig. 4E and fig. S7, A and B). Although the synthesis of *N*-carbamoyl-aspartate increased in response to insulin in CAD-S1859A mutant-expressing G9C cells, the labeling of pyrimidine intermediates downstream of CAD was not stimulated by insulin, with these metabolites detected at amounts similar to that in wild-type cells treated with the S6K1 inhibitor (Fig. 4E). These data suggest that the S6K1-mediated phosphorylation of S1859 enhances the *in vivo* dihydroorotase (E3) activity of CAD, with additional points of regulation from insulin and S6K1 possibly affecting upstream steps in the pathway (fig. S7C). The cells expressing CAD-S1859A were no longer acutely sensitive to insulin for the stimulated incorporation of de novo-synthesized pyrimidines into RNA and DNA (fig. S7D).

This study demonstrates that mTORC1 serves as a molecular link between growth signals and acute control over pyrimidine synthesis. It is worth emphasizing that mTORC1 and S6K1 are not essential for de novo pyrimidine synthesis *per se* but are required to increase flux through this pathway in response to growth-promoting signals,

such as insulin and nutrients. The direct regulation of CAD by S6K1 serves as a mechanism to increase the pool of nucleotides available for the RNA and DNA synthesis that accompanies cell growth. In addition to protein and lipid synthesis, pyrimidine synthesis represents another major anabolic process that is responsive to changes in cellular growth conditions through mTORC1 signaling.

References and Notes

1. M. Laplante, D. M. Sabatini, *Cell* **149**, 274 (2012).
2. V. Iadevaia, Y. Huo, Z. Zhang, L. J. Foster, C. G. Proud, *Biochem. Soc. Trans.* **40**, 168 (2012).
3. T. Porstmann *et al.*, *Cell Metab.* **8**, 224 (2008).
4. K. Düvel *et al.*, *Mol. Cell* **39**, 171 (2010).
5. J. Huang, B. D. Manning, *Biochem. J.* **412**, 179 (2008).
6. S. Menon, B. D. Manning, *Oncogene* **27**, (Suppl 2), S43 (2008).
7. A. Radu, V. Neubauer, T. Akagi, H. Hanafusa, M. M. Georgescu, *Mol. Cell Biol.* **23**, 6139 (2003).
8. M. Mori, M. Tatibana, *Methods Enzymol.* **51**, 111 (1978).
9. R. A. Williamson *et al.*, *Transplant. Proc.* **28**, 3088 (1996).
10. E. A. Carrey, D. G. Campbell, D. G. Hardie, *EMBO J.* **4**, 3735 (1985).
11. P. P. Hsu *et al.*, *Science* **332**, 1317 (2011).
12. Y. Yu *et al.*, *Science* **332**, 1322 (2011).
13. H. Flotow, G. Thomas, *J. Biol. Chem.* **267**, 3074 (1992).

14. D. R. Alessi, F. B. Caudwell, M. Andjelkovic, B. A. Hemmings, P. Cohen, *FEBS Lett.* **399**, 333 (1996).
15. L. R. Pearce *et al.*, *Biochem. J.* **431**, 245 (2010).
16. C. C. Dibble, J. M. Asara, B. D. Manning, *Mol. Cell Biol.* **29**, 5657 (2009).
17. L. M. Graves *et al.*, *Nature* **403**, 328 (2000).
18. L. A. Musmanno, R. S. Jamison, R. S. Barnett, E. Buford, J. N. Davidson, *Somat. Cell Mol. Genet.* **18**, 309 (1992).

Acknowledgements: We thank M. Yuan and S. Breitkopf for technical assistance with MS/MS and D. Patterson, D. Kwiatkowski, and M. Zbinden for cell lines. This work was supported in part by a grant from the LAM Foundation (I.B.-S.); NIH grants F32-DK095508 (J.J.H.), P01-CA120964 (B.D.M. and J.M.A.), and R01-CA122617 (B.D.M.); Dana Farber/Harvard Cancer Center grant P30-CA006516 (J.M.A.); and a Sanofi Innovation Award (B.D.M.). I.B.-S. and J.J.H. conceived and performed all experiments, analyzed all experimental data, and prepared the manuscript. J.M.A. performed and analyzed the MS/MS experiments. B.D.M. directed the research, reviewed all experimental data, and prepared the manuscript. All authors have reviewed the manuscript and declare no competing financial interests.

Supplementary Materials

www.sciencemag.org/cgi/content/full/science.1228792/DC1
Materials and Methods
Figs. S1 to S7
Tables S1 to S4
References (19–23)

13 August 2012; accepted 25 January 2013
Published online 21 February 2013;
10.1126/science.1228792

Proteomic Mapping of Mitochondria in Living Cells via Spatially Restricted Enzymatic Tagging

Hyun-Woo Rhee,^{1*†} Peng Zou,^{1*} Namrata D. Udeshi,² Jeffrey D. Martell,¹ Vamsi K. Mootha,^{2,3,4} Steven A. Carr,² Alice Y. Ting^{1,2‡}

Microscopy and mass spectrometry (MS) are complementary techniques: The former provides spatiotemporal information in living cells, but only for a handful of recombinant proteins at a time, whereas the latter can detect thousands of endogenous proteins simultaneously, but only in lysed samples. Here, we introduce technology that combines these strengths by offering spatially and temporally resolved proteomic maps of endogenous proteins within living cells. Our method relies on a genetically targetable peroxidase enzyme that biotinylates nearby proteins, which are subsequently purified and identified by MS. We used this approach to identify 495 proteins within the human mitochondrial matrix, including 31 not previously linked to mitochondria. The labeling was exceptionally specific and distinguished between inner membrane proteins facing the matrix versus the intermembrane space (IMS). Several proteins previously thought to reside in the IMS or outer membrane, including protoporphyrinogen oxidase, were reassigned to the matrix by our proteomic data and confirmed by electron microscopy. The specificity of peroxidase-mediated proteomic mapping in live cells, combined with its ease of use, offers biologists a powerful tool for understanding the molecular composition of living cells.

We sought to develop a method that circumvents the limited specificity and loss of material associated with organelle purification in traditional mass spectrometry (MS)-based proteomics. Our approach involves tagging the proteome of interest with a chemical handle such as biotin while the cell

is still alive, with all membranes, complexes, and spatial relationships preserved. Thus, we required a genetically targetable labeling enzyme that covalently tags its neighbors, but not more distant proteins, in living cells. One candidate is promiscuous biotin ligase (*I*-3), but its labeling is extremely slow (requiring 24

hours) (fig. S1) (*I*, 2), and the proposed mechanism proceeds through a biotin-adenylate ester, which has a half-life of minutes, implying a large labeling radius. Horseradish peroxidase (HRP)-catalyzed nitrene generation is another possibility (*4*), but we were unable to detect this labeling (fig. S2), and HRP is inactive when expressed in the mammalian cytosol (*5*).

We recently introduced engineered ascorbate peroxidase (APEX) as a genetic tag for electron microscopy (EM) (*5*). Unlike HRP, APEX is active within all cellular compartments. In addition to catalyzing the H₂O₂-dependent polymerization of diaminobenzidine for EM contrast, APEX also oxidizes numerous phenol derivatives to phenoxyl radicals. Such radicals are short lived (<1 ms) (*6*, *7*), have a small labeling radius (<20 nm) (*8*, *9*), and can covalently react with electron-rich amino acids such as Tyr, Trp, His, and Cys (*10–13*). This chemistry forms the basis of tyramide signal amplification (*14*), but it has not been extended to living cells.

¹Department of Chemistry, Massachusetts Institute of Technology (MIT), Cambridge, MA 02139, USA. ²Broad Institute of MIT and Harvard, Cambridge, MA 02142, USA. ³Department of Molecular Biology, Massachusetts General Hospital, Boston, MA 02115, USA. ⁴Department of Systems Biology, Harvard Medical School, Boston, MA 02115, USA.

*These authors contributed equally to this work.

†Present address: Ulsan National Institute of Science and Technology, Ulsan, Korea.

‡To whom correspondence should be addressed. E-mail: ating@mit.edu

To examine whether APEX could be employed for proteomic labeling (Fig. 1A), we targeted APEX to the mitochondrial matrix of human embryonic kidney (HEK) cells and initiated labeling by adding biotin-phenol and 1 mM H₂O₂ to the cell medium. Labeling was terminated after 1 min by cell fixation or lysis. Imaging by confocal microscopy (Fig. 1B) or stochastic optical reconstruction microscopy (STORM) (Fig. 1C) (15) showed that biotinylated proteins overlapped tightly with the mito-APEX construct. Streptavidin blot analysis of cell lysates showed that numerous endogenous proteins were biotinylated in an APEX- and H₂O₂-dependent manner (Fig. 1D and fig. S3).

To test the generality of our approach, we also analyzed other constructs that target APEX to different cellular regions (figs. S4 and S5). Seven different cytosol-facing APEX fusions gave distinct “fingerprints” in a streptavidin blot analysis, suggesting that targeted APEX biotinylates only a subset of cytosolic proteins, probably those in its close vicinity. We performed additional experiments to characterize the small-molecule specificity of APEX (fig. S2), the membrane permeability of the phenoxyl radical (fig. S6), and

the covalent adducts formed with amino acids in vitro (fig. S7; see also supplementary materials and methods).

We used mitochondrial matrix-targeted APEX to perform a proteomic experiment. Though mitochondria have been extensively characterized by MS proteomics, all previous studies have used mitochondrial purification, which is associated with sample loss and contamination. Consequently, the most comprehensive inventory of mitochondrial proteins (16) integrates MS proteomic data with green fluorescent protein imaging and computational analysis. Furthermore, proteome-scale maps of the matrix subcompartment in mammalian cells contain only a small number of proteins (17), representing very low coverage, probably because of the challenge of enriching for this subcompartment.

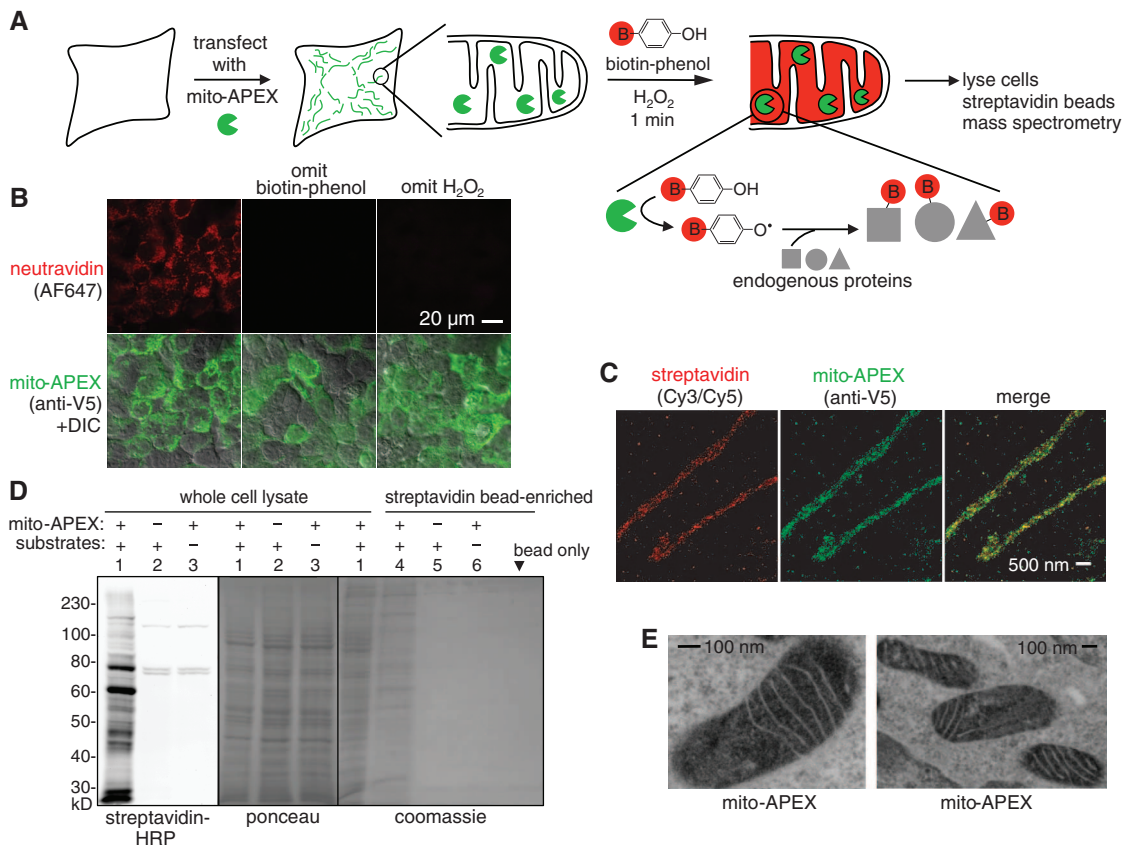
Endogenous proteins biotinylated by mito-APEX for 1 min in live HEK cells (as in Fig. 1) were purified using streptavidin beads, digested to peptides, and identified by tandem MS. We used stable isotope labeling (18) of experimental and control samples to distinguish between biotinylated proteins and nonspecific binders (fig. S8). We performed two independent replicates, each of

which produced a bimodal distribution of proteins based on isotope ratio (fig. S8C). The high-ratio distributions were strongly enriched for mitochondrial proteins, so we separated these hits and intersected the results from both replicates to obtain a list of 495 proteins (table S1), which we call our “matrix proteome.” This list is expected to contain both soluble matrix proteins and inner mitochondrial membrane (IMM) proteins that contact the matrix space.

Crossing our matrix proteome with earlier literature revealed that it was highly enriched for both mitochondrial and mitochondrial matrix proteins (Fig. 2A). Ninety-four percent (464 proteins) had prior mitochondrial annotation, leaving 31 “mitochondrial orphans” without any previously known connection to mitochondria (table S2). To further quantify the specificity of our matrix proteome, we examined the components of the electron-transport chain (Fig. 2C) and the TOM/TIM/PAM protein-import pathway (Fig. 2D), because they are structurally and/or topologically well characterized. In our matrix proteome, we detected only those subunits with exposure to the matrix space, illustrating the specificity and membrane-impermeability of our tagging.

Fig. 1. Labeling the mitochondrial matrix proteome in living cells.

(A) Labeling scheme. The APEX peroxidase was genetically targeted to the mitochondrial matrix via fusion to a 24-amino acid targeting peptide (5). Labeling was initiated by the addition of biotin-phenol and H₂O₂ to live cells for 1 min. Cells were then lysed, and biotinylated proteins were recovered with streptavidin-coated beads, eluted, separated on a gel, and identified by MS. The peroxidase-generated phenoxyl radical is short-lived and membrane-impermeant and, hence, covalently tags only neighboring and not distant endogenous proteins. B, biotin. **(B)** Confocal fluorescence imaging of biotinylated proteins (stained with neutravidin) after live labeling of HEK cells expressing mito-APEX as in (A). Controls were performed with either biotin-phenol or H₂O₂ omitted. DIC, differential interference contrast. **(C)** Superresolution STORM images showing streptavidin and APEX (AF405/AF647) localization patterns at 22-nm resolution in U2OS cells. Samples were reacted as in (B). **(D)** Gel analysis of biotinylated mitochondrial matrix proteins, before (lanes 1 to 3) and after (lanes 4 to 6) streptavidin bead enrichment. Samples were labeled as in (B). Substrates are biotin-phenol and H₂O₂. Mammalian cells have four endogenously biotinylated proteins, three of which were observed in the negative con-



control lanes (2 and 3) of the streptavidin blot. **(E)** Electron microscopy of HEK cells expressing mito-APEX. EM contrast was generated by treating fixed cells with H₂O₂ and diaminobenzidine. APEX catalyzes the polymerization of diaminobenzidine into a local precipitate, which is subsequently stained with electron-dense OsO₄ (5). Dark contrast is apparent in the mitochondrial matrix, but not the intermembrane space.

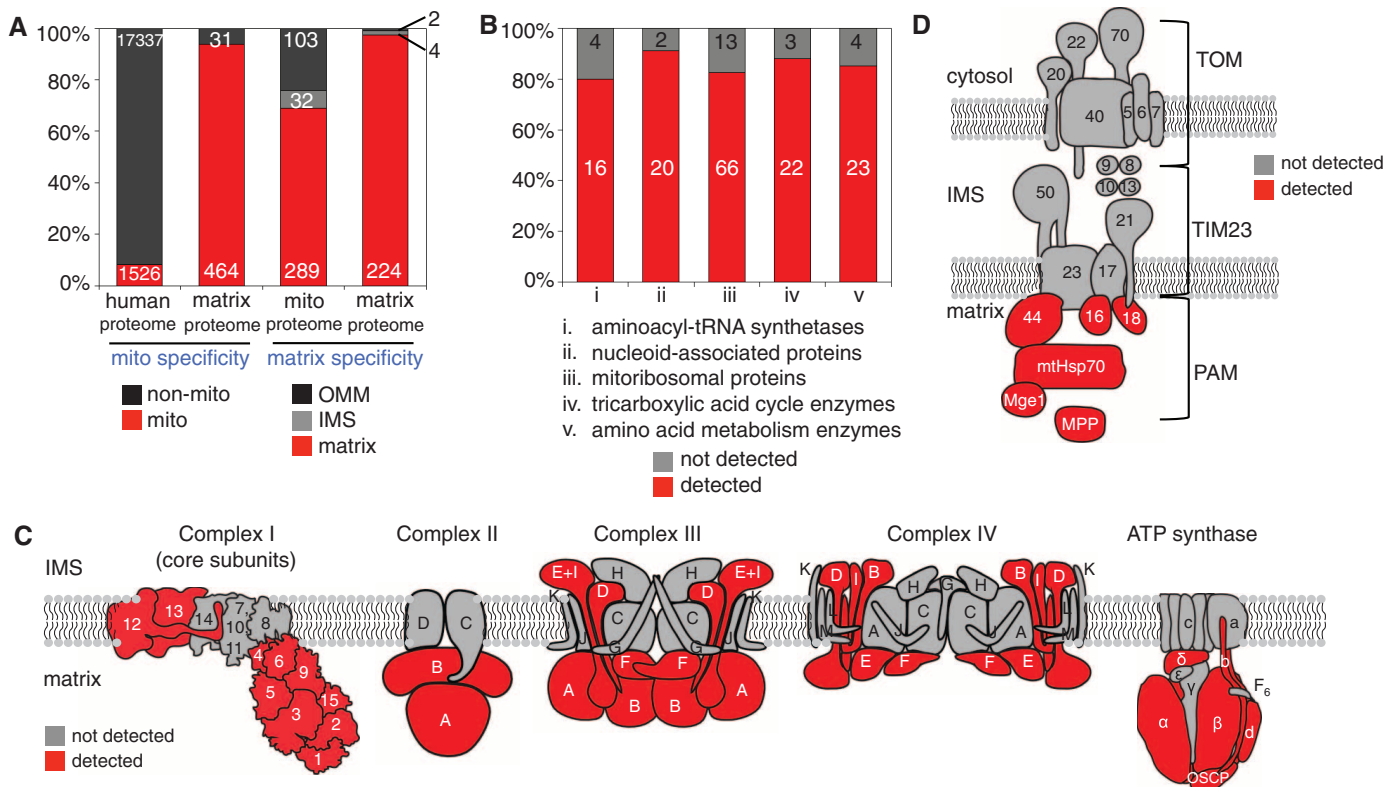


Fig. 2. Specificity and depth of coverage of the mitochondrial matrix proteome. **(A)** Analysis of specificity. The left two columns show the fraction of proteins with prior mitochondrial annotation in the entire human proteome (column 1) and in our matrix proteome (column 2). The right two columns show the distribution of proteins with prior submitochondrial localization information, for all mitochondrial proteins (column 3) and for our matrix proteome (column 4). See table S6 for details. **(B)** Analysis of depth of coverage. Five groups of well-established mitochondrial matrix proteins (i to v) were crossed with our proteomic list. For each group, 80 to 91% of proteins were detected in our matrix proteome. See table S7 for details. **(C)** Analysis of labeling specificity

for protein complexes of the IMM. The subunits of complexes I to IV and F_0F_1 adenosine triphosphate (ATP) synthase, for which structural information is available, are illustrated. Subunits detected in our matrix proteome are shaded red; those not detected are shaded gray. Note that because structural information is not available for all 45 subunits of complex I, some subunits that appear exposed here may not be exposed in the complete complex. OSCP, oligomycin sensitivity conferral protein. **(D)** Same analysis as in (C), for proteins of the TOM/TIM/PAM protein-import machinery that span the OMM and IMM. All proteins depicted in (C) and (D) are listed, with additional information, in table S8.

To analyze depth of coverage, we checked our matrix proteome for well-established groups of soluble matrix proteins (Fig. 2B). We detected members of each group at a rate of 80 to 90% and found nearly identical subsets of proteins in each of the two replicates, suggesting that coverage was high, but for only ~85% of proteins. The proteins we consistently did not detect were not low-abundance proteins (fig. S8F), nor did they lack surface-exposed tyrosine residues. We hypothesize that these proteins were sterically buried in macromolecular complexes, making them inaccessible to the phenoxyl radical.

For a subset of proteins in our proteome, we detected directly biotinylated peptides (fig. S9 and table S4). Tandem MS sequencing showed that biotin-phenol was conjugated to tyrosine side chains. In nearly all cases, the biotinylated tyrosine residue mapped to a surface-exposed site on a soluble protein or a matrix-exposed site on a transmembrane protein.

Our matrix proteome of 495 proteins provides a number of interesting insights. First, the 31 mitochondrial orphans may be newly discovered mitochondrial proteins. We selected and

imaged six of these at random and found complete or partial mitochondrial localization for all of them (fig. S10). Second, 240 proteins with unknown submitochondrial localization can now be assigned by our data to the matrix compartment (table S3). Third, we detected six proteins previously assigned to the intermembrane space (IMS) or outer mitochondrial membrane (OMM): PPOX, CPOX, PNPT1, CHCHD3, COASY, and SAMM50. To determine if our detection of these proteins in the matrix was accurate, we performed EM imaging, taking advantage of APEX's additional functionality as an EM tag (5). APEX fusions to five of the six proteins showed matrix staining by EM (Fig. 3 and fig. S11). We were unable to examine the final protein, SAMM50, because APEX insertion at four different sites abolished mitochondrial targeting.

The proteins PPOX and CPOX are particularly interesting in this group because they catalyze two of the later steps in heme biosynthesis (Fig. 3A). Previous studies on purified mitochondria or mitoplasts treated with proteases or membrane-impermeant inhibitors have localized both enzymes to the IMS (19–22). Structural anal-

ysis and modeling have indicated that PPOX docks to ferrochelatase (FECH), the final iron-inserting enzyme of heme biosynthesis, through the IMM (23) (Fig. 3F). This model is inconsistent with our EM data, because we found that both the C terminus and amino acid 205 of PPOX localize to the matrix (Fig. 3C). Our EM data on CPOX, on the other hand, are consistent with previous literature, because we found that residue 70 localizes to the matrix (explaining the detection of CPOX in our matrix proteome), whereas the C terminus and residue 120 flanking the active site localize to the IMS (Fig. 3D). Our reassignment of PPOX from the IMS to the matrix has implications for the nature of its interactions with CPOX and FECH and the mechanisms by which its substrates are transported across the IMM.

We have developed a method for mapping the proteomic composition of cellular organelles, using a genetically targetable peroxidase that catalyzes the generation of short-lived, highly reactive, and membrane-impermeant radicals in live cells. With a temporal resolution of 1 min, labeled proteins are harvested and identified by

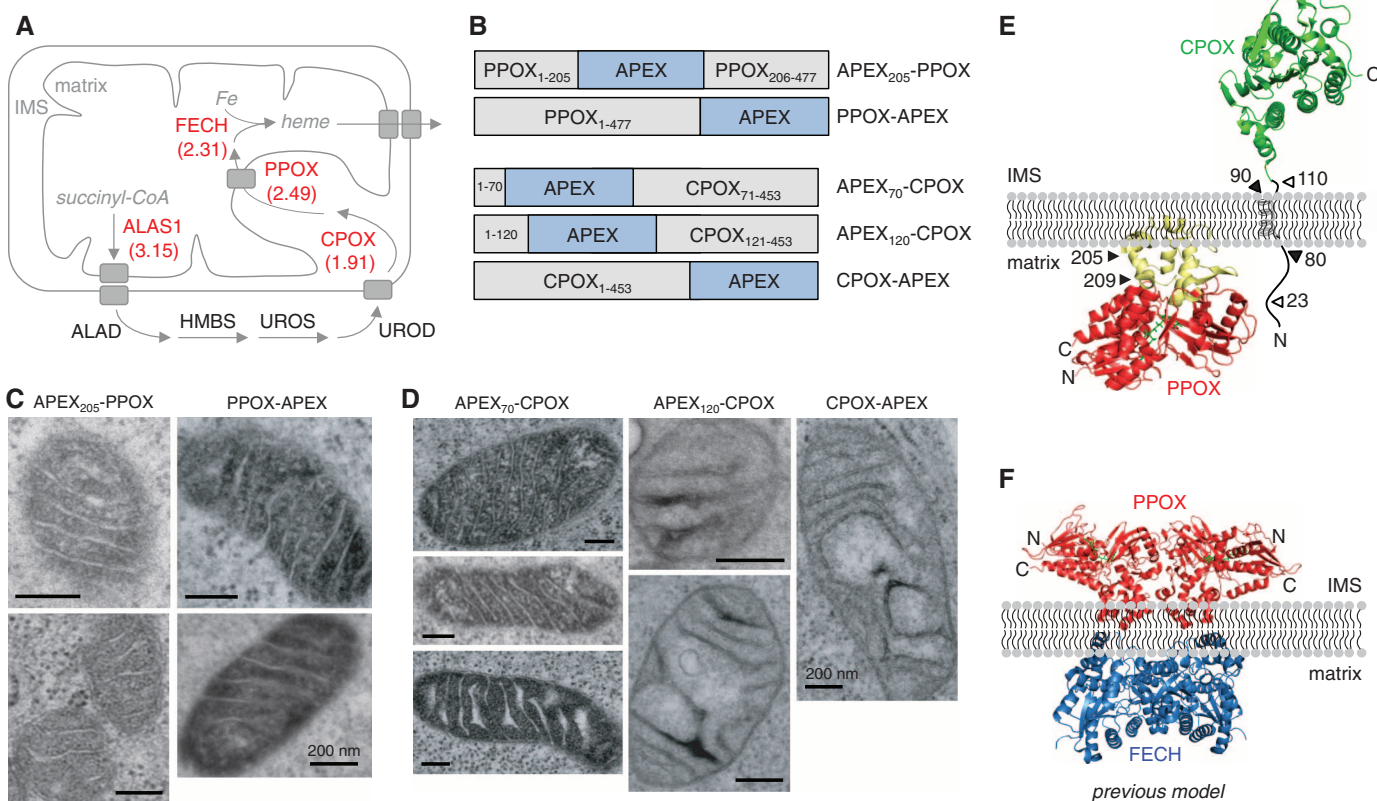


Fig. 3. Submitochondrial localization of the heme biosynthesis enzymes CPOX and PPOX. **(A)** Model showing the submitochondrial localizations of the eight core enzymes that catalyze heme biosynthesis, according to previous literature (24). Four of these enzymes are detected in our matrix proteome and are shown in red [with log₂(heavy/light) ratios from replicate 1. CoA, coenzyme A. Drawing adapted from (25). **(B)** Domain structures of PPOX and CPOX fusions to APEX, imaged by EM in **(C)** and **(D)**, respectively. Additional EM images of PPOX-APEX are shown in fig. S11B. Scale bars in **(C)** and **(D)**,

200 nm. **(E)** Our model for PPOX and CPOX localization, based on our EM data and previous literature (19–22). The predicted membrane-binding region of PPOX (residues 92 to 209) is shown in yellow (26). Hollow arrowheads point to predicted cleavage sites in CPOX. **(F)** Previous model showing the docking of a PPOX dimer and a FECH dimer through the IMM (23). N- and C-terminal ends of PPOX are labeled. Our data contradict this model, because the EM images in **(C)** show that the C terminus and residue 205 of PPOX are in the matrix, not the IMS.

MS with the use of well-established techniques. In addition to its simplicity, our method has no noticeable toxicity, requires far less material than conventional organellar proteomics, and takes hours to implement rather than days (as for sub-cellular fractionation). Our initial demonstration on the human mitochondrial matrix proteome shows that specificity is exceptionally high because labeling is performed in living cells while membranes and other structures are still intact. Depth of coverage is also high for the majority of proteins—most likely those that are sterically accessible to the phenoxyl radical. Notably, our method provides insight into the topology of identified proteins. Finally, the same peroxidase, APEX, can be used for both proteomic mapping and EM visualization (5).

References and Notes

1. K. J. Roux, D. I. Kim, M. Raida, B. Burke, *J. Cell Biol.* **196**, 801 (2012).
2. B. Morriswood *et al.*, *Eukaryot. Cell* **12**, 356 (2013).
3. E. Choi-Rhee, H. Schulman, J. E. Cronan, *Protein Sci.* **13**, 3043 (2004).
4. N. Kotani *et al.*, *Proc. Natl. Acad. Sci. U.S.A.* **105**, 7405 (2008).
5. J. D. Martell *et al.*, *Nat. Biotechnol.* **30**, 1143 (2012).

6. J. F. Wishart, B. S. Madhava Rao, in *Recent Trends in Radiation Chemistry* (World Scientific, Singapore, 2010), pp. 577–596.
7. A. Mortensen, L. H. Skibsted, *J. Agric. Food Chem.* **45**, 2970 (1997).
8. M. Bendayan, *Science* **291**, 1363 (2001).
9. G. Mayer, M. Bendayan, *J. Histochem. Cytochem.* **45**, 1449 (1997).
10. K. Minamihata, M. Goto, N. Kamiya, *Bioconjug. Chem.* **22**, 2332 (2011).
11. M. S. Rogers *et al.*, *Biochemistry* **47**, 10428 (2008).
12. B. Bhaskar *et al.*, *J. Mol. Biol.* **328**, 157 (2003).
13. F. Amini, T. Kodadek, K. C. Brown, *Angew. Chem. Int. Ed. Engl.* **41**, 356 (2002).
14. W. Schönhuber, B. Fuchs, S. Juretschko, R. Amann, *Appl. Environ. Microbiol.* **63**, 3268 (1997).
15. B. Huang, M. Bates, X. Zhuang, *Annu. Rev. Biochem.* **78**, 993 (2009).
16. D. J. Pagliarini *et al.*, *Cell* **134**, 112 (2008).
17. F. Forner, L. J. Foster, S. Campanaro, G. Valle, M. Mann, *Mol. Cell. Proteomics* **5**, 608 (2006).
18. S. E. Ong *et al.*, *Mol. Cell. Proteomics* **1**, 376 (2002).
19. G. C. Ferreira, T. L. Andrew, S. W. Karr, H. A. Dailey, *J. Biol. Chem.* **263**, 3835 (1988).
20. J.-C. Deybach, V. da Silva, B. Grandchamp, Y. Nordmann, *Eur. J. Biochem.* **149**, 431 (1985).
21. G. H. Elder, J. O. Evans, *Biochem. J.* **172**, 345 (1978).
22. B. Grandchamp, N. Phung, Y. Nordmann, *Biochem. J.* **176**, 97 (1978).
23. M. Koch *et al.*, *EMBO J.* **23**, 1720 (2004).
24. I. Hamza, H. A. Dailey, *Biochim. Biophys. Acta Mol. Cell Res.* **1823**, 1617 (2012).

25. R. Nilsson *et al.*, *Cell Metab.* **10**, 119 (2009).
26. X. Qin *et al.*, *FASEB J.* **25**, 653 (2011).

Acknowledgments: We thank N. Watson (Whitehead Institute Keck Microscopy Facility) and E. Vasilie (Koch Institute Microscopy Core Facility) for performing EM imaging, H. B. Fraser for assistance with data analysis and manuscript editing, C. Uttamapinant for piocoyl azide-AF647, X. Zhuang and her lab for advice on STORM, H. A. Dailey for advice on CPOX and PPOX, and S. Calvo for assistance with data analysis. Funding was provided by the NIH (grants DP1 OD003961 to A.Y.T. and R01 GM077465 to V.K.M.), the Dreyfus Foundation (A.Y.T.), the American Chemical Society (A.Y.T.), and the Broad Institute of MIT and Harvard (S.A.C.). The authors have no conflicting financial interests. A patent application relating to the use of enzymes for proteomic mapping in live cells has been filed by MIT. Proteomic data can be found in supplementary tables S1 to S9. The authors will make the genetic constructs used in this work widely available to the academic community through Addgene (www.addgene.org).

Supplementary Materials

www.sciencemag.org/cgi/content/full/science.1230593/DC1
Materials and Methods
Figs. S1 to S11
Tables S1 to S9
References (27–53)

24 September 2012; accepted 11 January 2013
Published online 31 January 2013;
10.1126/science.1230593